Thrust Evaluation of Small-Scale Magnetic Sail Spacecraft by Three-Dimensional Particle-in-Cell Simulation

AUTHOR(S):

Ashida, Yasumasa; Yamakawa, Hiroshi; Funaki, Ikkoh; Usui, Hideyuki; Kajimura, Yoshihiro; Kojima, Hirotsugu

Thrust Evaluation of Small-Scale Magnetic Sail Spacecraft by Three-Dimensional Particle-in-Cell Simulation

Yasumasa Ashida[1]
Kyoto University, Uji, Kyoto 611-0011, Japan

Hiroshi Yamakawa[2]
Kyoto University, Uji, Kyoto 611-0011, Japan

Ikkoh Funaki[3]
Japan Aerospace Exploration Agency, Sagamihara, Kanagawa 252-5210, Japan

Hideyuki Usui[4]
Kobe University, Kobe, Hyogo 657-8501, Japan

Yoshihiro Kajimura[5]
Akashi National College of Technology, Akashi, Hyogo 674-8501, Japan

and
Hirotsugu Kojima[6]
Kyoto University, Uji, Kyoto 611-0011, Japan

A magnetic sail is a spacecraft propulsion system that generates an artificial magnetosphere to block solar wind particles and uses the imparted momentum to accelerate a spacecraft. In the present study, we conducted three-dimensional particle-in-cell simulations on small-scale magnetospheres to investigate the thrust characteristics of small-scale magnetic sails. The results show that electron Larmor motion and charge separation become significant in small-scale magnetospheres, and that the thrust of the magnetic sail is affected by the cross-sectional area of the charge-separated plasma cavity. Empirical formulae for the thrust are obtained by changing spacecraft design and solar wind parameters. These equations show that the thrust of small-scale magnetic sail is approximately proportional to magnetic moment, solar wind density and solar wind velocity.

---

[1] Graduate student, Division of Creative Research and Development of Humanosphere, Research Institute for Sustainable Humanosphere, Gokasho.
[2] Professor, Division of Creative Research and Development of Humanosphere, Research Institute for Sustainable Humanosphere, Gokasyo, Senior Member AIAA.
[3] Associate Professor, Institute of Space and Astronautical Science, 3-1-1 Yoshinodai, Senior Member AIAA.
[4] Professor, Graduate School of System Informatics, 1-1 Rokkodai, Nada.
[5] Lecturer, Department of Electric and Computer Engineering, 679-3 Nisioka, Uozumi-cho, Member AIAA.
[6] Associate Professor, Division of Creative Research and Development of Humanosphere, Research Institute for Sustainable Humanosphere, Gokasho.

The empirical formulae enable us to determine the trajectory of the spacecraft and perform a mission analysis.

Nomenclature

B	=	magnetic flux vector, T
B_{MP}	=	magnetic flux density at magnetopause, T
c	=	speed of light, m/s
dt	=	time step, s
dx	=	grid spacing, m
E	=	electric field vector, V/m
e	=	elementary charge, C
F	=	thrust force of magnetic sail, N
G	=	gravitational constant, $6.67\text{x}10^{-11}$ $m^3/s^2 \cdot kg$
J	=	current density vector, A/m^2
L_{MHD}	=	analytical magnetosphere size calculated under MHD approximation, m
L_s	=	plasma cavity size defined by stagnation point, m
M	=	magnetic moment of coil, Wb·m
m_e	=	mass of electron, kg
m_i	=	mass of ion, kg
N_{SW}	=	number density of solar wind, m^{-3}
n_e	=	number density of electrons, m^{-3}
n_i	=	number density of ions, m^{-3}
q_i	=	charge of ion, $+e$ C
q_e	=	charge of electron, $-e$ C
r	=	position vector of plasma particle, m
r_L	=	Larmor radius, m
T_{SW}	=	solar wind temperature, K
V_{SW}	=	velocity of solar wind, m/s

$\mathbf{v}$ = velocity vector of plasma particle, m/s

I. Introduction

A MAGNETIC sail is a spacecraft propulsion system aimed at fast interplanetary flight for deep space exploration. Zubrin and Andrews first proposed the concept of a magnetic sail in 1991 [1]. They designed a conceptual spacecraft having a large loop of superconducting coil (Fig. 1). This onboard superconducting coil produces an artificial magnetic cavity (magnetosphere) that reflects approaching solar wind particles. Through this interaction, the solar wind flow loses momentum and a corresponding repulsive force is exerted on the coil to accelerate the magnetic sail spacecraft away from the Sun without consuming fuel or electric power. The specific impulse and thrust/power ratio of a magnetic sail are therefore infinite. Interest was renewed in the idea of the magnetic sail when Winglee et al. proposed the idea of creating a large magnetosphere by combining a compact coil (diameter of several meters) with a plasma jet [2] instead of using the large coil (diameter of several kilometers) proposed by Zubrin. This propulsion system is called mini-magneto plasma propulsion (M2P2) or a magneto plasma sail (MPS).

Several numerical simulations have been performed to examine the thrust characteristics of the magnetic sail. Nishida et al. [3] revealed the thrust generation mechanism of a magnetic sail by performing ideal magnetohydrodynamics (MHD) simulations of a very large magnetosphere in which the finite ion Larmor radius effect is neglected. When this effect must be considered and the electrons can be assumed to be a fluid in the magnetosphere (>100 km), hybrid particle-in-cell (PIC) simulations are used. Hybrid-PIC simulations treat ions as particles and electrons as a fluid. Fujita [4] evaluated the effects of ion kinetics on thrust in magnetospheres of various sizes, and Kajimura et al. [5] performed similar hybrid-PIC simulations with the goal of reproducing certain experimental results [6]. In addition, we developed a flux tube simulation method for quickly and accurately evaluating the thrust of a magnetic sail in spacecraft design [7]. These studies elucidated the thrust characteristics of magnetic sails that have a large magnetosphere (>100 km). These simulation techniques are currently being used to evaluate M2P2/MPS systems, which inflate the magnetosphere of the original magnetic sail using a plasma jet from the spacecraft to obtain a larger thrust [8, 9, 10, 11, 12].

However, the thrust of a magnetic sail has not been evaluated for a small-scale magnetosphere (<100 km), which is feasible using present superconductive technology and launch capabilities of rockets. It is, therefore, uncertain whether missions to demonstrate thrust generation are realizable. The difficulty is that the kinetic effects of electrons must be considered in such a small-scale magnetosphere, and neither MHD simulation nor hybrid-PIC simulation is

suitable for doing so [13]. Full-PIC simulation, which treats both ions and electrons as particles, is needed in order to take into account the particle nature of plasma, including finite Larmor radius effects and charge separation. Moritaka et al. [14] simulated the momentum transfer of the solar wind in two dimensions by using the artificial mass ratio, $m_i/m_e = 25$. We have also calculated the thrust of magnetic sails in two dimensions with the realistic mass ratio, $m_i/m_e = 1836$ [15], and identified the charge-separated magnetosphere and the finite thrust generation of an M2P2/MPS system that is competitive with existing propulsion systems. However, no one has successfully modeled the thrust of an M2P2/MPS system in three dimensions by performing full-PIC simulation. Mission design and spacecraft design require three-dimensional full-PIC simulations, which entail very large computational costs, since the true thrust characteristics of magnetic sails cannot be fully determined by two-dimensional analysis alone. Although large three-dimensional full-PIC simulations have recently become possible owing to improvements in parallel computing techniques, computing power is still insufficient for simultaneously analyzing the completely different phenomena of the formation of the magnetosphere and magnetic expansion.

The objective of the present study is to model the thrust characteristics of magnetic sails that have small-scale magnetospheres ranging from hundreds of meters to several kilometers by performing full-PIC simulations in three dimensions. We focus on the fundamental thrust characteristics of magnetic sails, ignoring magnetic expansion. Empirical formulae for the thrust will be obtained by simulations with various spacecraft designs and solar wind parameters. These will enable us to design missions and discuss the feasibility of the magnetic sail based on realistic thrust values without making any unnecessary assumptions.

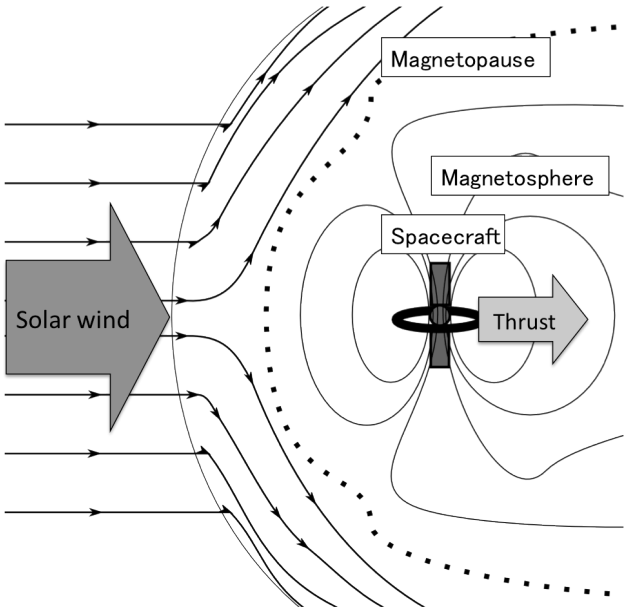

Fig. 1 Schematic illustration of a magnetic sail and the magnetosphere formed by the interaction between an onboard spacecraft coil and the solar wind.

II. Numerical Model for Full-PIC Simulation

The magnetosphere's size in the MHD approximation (single-fluid approximation) is derived from the balance between the magnetic pressure and the dynamic pressure of the solar wind [16]:

$$L_{MHD} = \left(\frac{\mu_0 M^2}{16\pi^2 N_{SW} m_i V_{SW}^2} \right)^{\frac{1}{6}} \quad (1).$$

When the magnetosphere's size is comparable to the ion Larmor radius ($L_{\mathrm{MHD}} \sim R_{\mathrm{iL}}$), the ion kinetics should be considered. When L_{MHD} is smaller than R_{iL} and comparable to the electron Larmor radius ($L_{\mathrm{MHD}} \sim R_{\mathrm{eL}}$), the electron kinetics should be considered. In addition, in such small magnetospheres, it is expected that the charge separation should be significant since the Debye length in the solar wind becomes comparable with the magnetosphere's size ($L_{\mathrm{MHD}} \sim \lambda_D$). We note that the calculated magnetosphere sizes for small-scale magnetic sails do not necessarily agree with L_{MHD} since the calculation of L_{MHD} was performed ignoring particle motion in the plasma, and a smaller magnetosphere is typically formed. Here, the typical values of the ion Larmor radius, electron Larmor radius and Debye length are 100 km, 50 m and 30 m, respectively. Hence, for a magnetosphere of size L_{MHD}<100 km (M<1.0 × 10^{14} Wb·m) the kinetic effects of plasma should be taken into consideration. We use a full kinetic simulation technique, called full-PIC simulation, to simulate the plasma flow in three dimensions around a magnetic sail.

Full-PIC simulation treats both ions and electrons as particles in order to consider the kinetic effects of plasma particles such as finite Larmor radius and charge separation. Full-PIC simulation solves the equation of motion

$$m_s \frac{d\mathbf{v}_s}{dt} = q_s \left(\mathbf{E} + \mathbf{v}_s \times \mathbf{B} \right) \quad s = \text{ion, electron} \quad (2),$$

and traces the precise motion of each particle using the Buneman-Boris method [17]. In this study, only two kinds of particles, namely, ions (protons) and electrons, are used and the mass ratio is fixed (m_i/m_e = 1836). When an artificial mass ratio is assumed, the thrust of magnetic sail and plasma phenomena cannot be reproduced correctly. The real mass ratio and realistic plasma parameters are required for the simulation of magnetic sails. From the particle trajectories, the density distribution and current distribution are calculated by the PIC weighting method. Maxwell's equations

$$\frac{\partial \mathbf{B}}{\partial t} = -\nabla \times \mathbf{E} \tag{3}$$

and

$$\frac{1}{c^2}\frac{\partial \mathbf{E}}{\partial t} = \nabla \times \mathbf{B} - \mu_0 \mathbf{J} \tag{4}$$

are solved by the finite-difference time-domain method to obtain a self-consistent electromagnetic field.

The interaction between the solar wind and an artificial dipole magnetic field is simulated in three-dimensional space. Figure 2 shows the computational domain used in the three-dimensional full-PIC simulations. The computational domain has an area of 3.8 km × 3.8 km × 3.8 km, which is partitioned into a grid of 256 × 256 × 256 cells ($dx = 15$ m) in the typical case. The size of the computational domain is chosen based on the theoretical magnetosphere size L_{MHD} (Eq. (1)): the length of one side is approximately $5L_{\mathrm{MHD}}$. The grid spacing dx typically needs to be chosen so that it is not much larger than the Debye length ($dx/\lambda_D < 3$). The time spacing dt must fill the Courant condition, $dx/dt > 1.73c$ in three-dimensions ($dt = 1.5 \times 10^{-8}$ s). The solar wind plasma is typically represented by 16 super particles associated with each cell and a total of 5.4×10^8 particles. This is because it was found in our previous study [15] that the number of particles per cell does not have as much influence on the precision of the thrust as the latitude resolution or the size of calculation domain. Sixteen particles are sufficient for an accurate simulation. The magnetic field generated by the coil mounted in the spacecraft is approximated by an ideal dipole magnetic field or a finite size coil magnetic field of magnetic moment M. The magnetic moment of the coil is arranged in the y-direction (perpendicular to the solar wind, Fig. 3a) or in the z-direction (parallel to the solar wind, Fig. 3b). The magnetic field is given as an initial condition and absorbing boundary conditions are used for the electromagnetic field on all outer boundaries. Solar wind particles flow into the computational domain from the inflow boundary with the typical solar wind velocity V_{SW} and thermal distribution. Particles leaving the computational domain are eliminated from the calculation. Collisions between particles and the spacecraft are also not taken into consideration.

The computational load for a full-PIC simulation to calculate the trajectory of huge numbers of plasma particles is very large. This has prevented the simulation of the plasma flow around small-scale magnetic sails to obtain thrust characteristics. However, large three-dimensional full-PIC simulations have recently become possible due to improvements in parallel computing techniques. We use the so-called hybrid parallelization technique that uses both

process parallelization and thread parallelization. As shown in Fig. 2a, the computational domain is divided into some smaller cuboids (8 × 8 × 256 cells in typical case) by domain decomposition. Calculations by MPI are performed separately in each small domain and bordering physical quantities are exchanged. Figure 2b shows one small computational domain. The domain includes a huge number of particles (approximately 0.5 million in a typical case). These particles are divided into groups by particle decomposition and each particle group is simulated in one OpenMP thread. As a result, 4096 CPUs (1024 MPI processes and 4 OpenMP threads) are used for the simulation. Figure 4 shows the calculation flow of our full-PIC code. The calculation is continued until a steady thrust is obtained. The thrust of a magnetic sail is calculated by the momentum change of the solar wind flow as

$$\mathbf{F}_{flow} = -\oint \left(m_i n_i \mathbf{u}_i \mathbf{u}_i + \frac{\mathbf{B}\cdot\mathbf{B}}{2\mu_0}\mathbf{I} - \frac{\mathbf{BB}}{\mu_0} \right) \cdot \mathbf{n}\, ds \tag{5}.$$

Note that $\mathbf{u}_i\mathbf{u}_i$, **BB** and **I** are tensors. The integration is performed in an arbitrary control volume. In previous studies [3, 7], it was confirmed that thrusts calculated from the change in momentum of particles, the electromagnetic force acting on the onboard coil or the momentum that passes through a control volume agree to within 10% in the steady state.

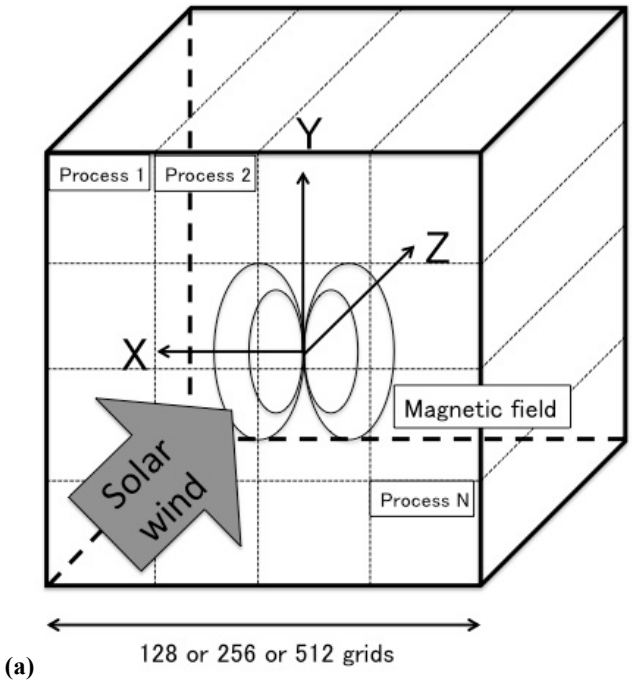

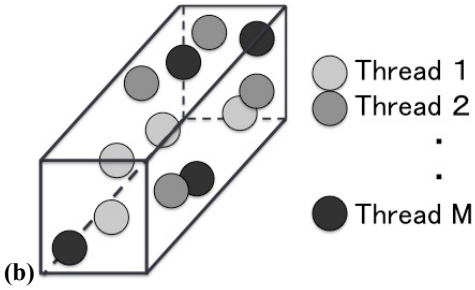

Fig. 2 Coordinate system adopted for three-dimensional full-PIC simulations. The solar wind direction is parallel to the z-axis.

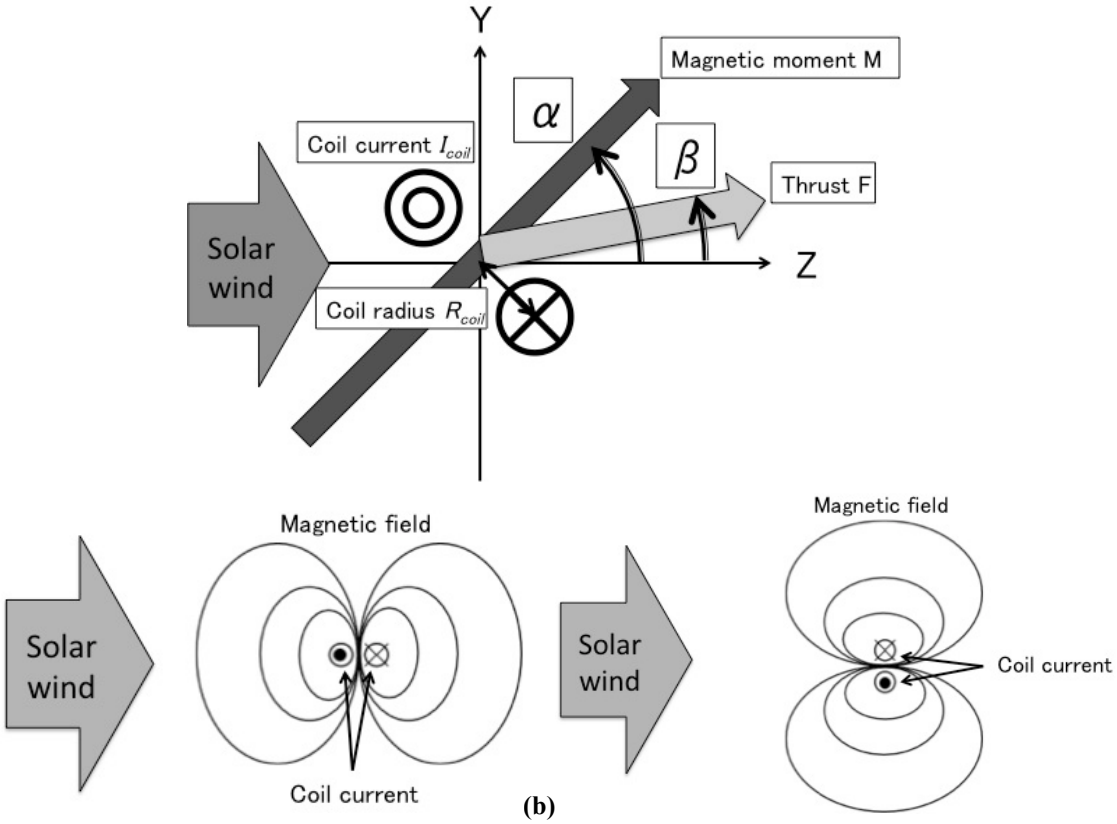

Fig. 3 Definition of attack angle α and steering angle β. Note that (a) is referred to as the perpendicular case (α = 90 deg) and (b) is referred to as the parallel case (α = 0 deg).

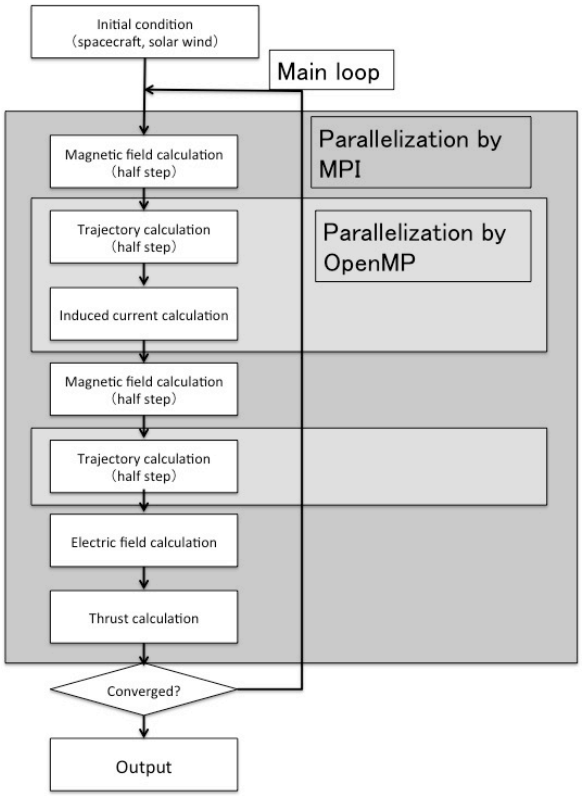

Fig. 4 Calculation flow of parallelized full-PIC simulation code.

III. Thrust Characteristics of Magnetic Sail

A. Structure of a typical small-scale magnetic sail

First, a three-dimensional magnetic sail was simulated using the typical solar wind parameters at Earth orbit (Table 1). For simplicity, direct collisions between particles are neglected in this paper. The interplanetary magnetic field can also be ignored, as revealed by two-dimensional full-PIC simulation [15] and MHD simulation [18]. Table 2 lists the design parameters of the magnetic sail; these parameters are expected to give a small-scale magnetic sail (on the order of 100 m) in which electron kinetic effects are significant.

Figures 5 and 6 show the spatial distribution of ion density in the steady state when the magnetic moment M is perpendicular to the solar wind ($\alpha = 90$ deg) and parallel to the solar wind ($\alpha = 0$ deg), respectively. It took about 4 days using 1024 CPUs to obtain the steady state plasma flow and approximately 100 GB of memory was required. In each of these figures, slices through the xz-plane (magnetic equatorial plane) and yz-plane (magnetic meridian plane) are shown as subfigures (a) and (c), respectively. One-dimensional cuts along the x-axis (y=0 m and z=0 m, 200 m, 400 m) and the y-axis (x=0 m, z=0 m, 200 m, 400 m) are also shown in subfigures (b) and (d), respectively. In both the perpendicular and parallel cases, a low-density region is formed around the spacecraft at (x, y, z) = (0, 0, 0) despite the loose coupling between the ions and magnetic field because of the large Larmor radius of the ions. In contrast to the results of simulations by MHD and the geophysical magnetosphere, this low-density region is accompanied by only a very weak discontinuity in the magnetic field since the plasma can induce a weak magnetopause current in small length scales. In this paper we therefore call the low-density region in the full-PIC simulations the plasma cavity instead of the magnetosphere. The thrust of a small-scale magnetic sail is caused by the formation of a plasma cavity in the same way that the thrust of a large-scale magnetic sail is caused by formation of a magnetosphere.

The plasma cavity is asymmetric about the yz-plane and symmetric about the xz-plane in the perpendicular case, since the Lorentz force on the ions is in the same direction for both $x > 0$ and $x < 0$ (Fig. 5). The cross-sectional area of the plasma cavity S is therefore approximately calculated from the product of the cross-sectional widths along the x-axis ($z = 400$ m) and y-axis ($z = 400$ m). We chose $z = 400$ m since the streamlines of the solar wind become almost straight at the point, as shown in Figs 5a and 5c. The cross-sectional width is calculated from the region where the ion density falls below the solar wind density (5×10^6 m^{-3}), as shown in Figs. 5b and 5d. The simulation results give $S = \pi \times (300/2)$ m $\times (350/2)$ m $= 8.2 \times 10^4$ m^2. In contrast, the plasma cavity in the parallel case is

symmetric about the z-axis, as shown in Fig. 6. As before, the cross-sectional area of the plasma cavity S is approximately calculated from the product of the cross-sectional widths along the x-axis (z = 400 m) and y-axis (z = 400 m) shown in Figs. 6b and 6d. The calculated cross-sectional area is $S = \pi \times (250/2\ \mathrm{m})^2 = 4.9 \times 10^4\ \mathrm{m}^2$. Note that the cross-sectional area is thus slightly larger, and thus can receive more momentum from the solar wind, in the perpendicular case than in the parallel case. The momentum of the solar wind then generates the thrust of the magnetic sail as a repulsive force between the magnetopause current and the coil current onboard the spacecraft. The current density distributions of both the perpendicular case and the parallel case are shown in Fig. 7. The magnetopause current induced by the solar wind plasma flows counter to the coil current. One-dimensional cuts of current density along y-axis (x=0 m, z=0 m, 200 m, 400 m) are also shown in Figs. 7b and 7d. It is expected that most of the thrust of the magnetic sail will be generated at the front of a plasma cavity since the current is strong at z=0 m. Moreover, the position where the magnetopause current flows is mostly in agreement with the position where plasma density is low.

The thrust of the magnetic sail was calculated from the change in momentum of all particles contained in the computational domain. The thrust in the perpendicular case (0.08 ± 0.008 mN) is larger than in the parallel case (0.07 ± 0.007 mN) because of the larger plasma cavity.

Table 1 Typical parameters of the solar wind

Solar wind velocity V_{SW} [m/s]	Solar wind density N_{SW} [m^{-3}]	Plasma temperature T_{SW} [eV]	Interplanetary magnetic field [T]
5×10^5	5×10^6	10	0 (ignored)

Table 2 Magnetic sail design parameters

Magnetic moment M [Wb·m]	Magnetic moment direction	Coil radius [m]
1.3×10^8	y-direction (perpendicular case) and z-direction (parallel case)	0 (dipole)

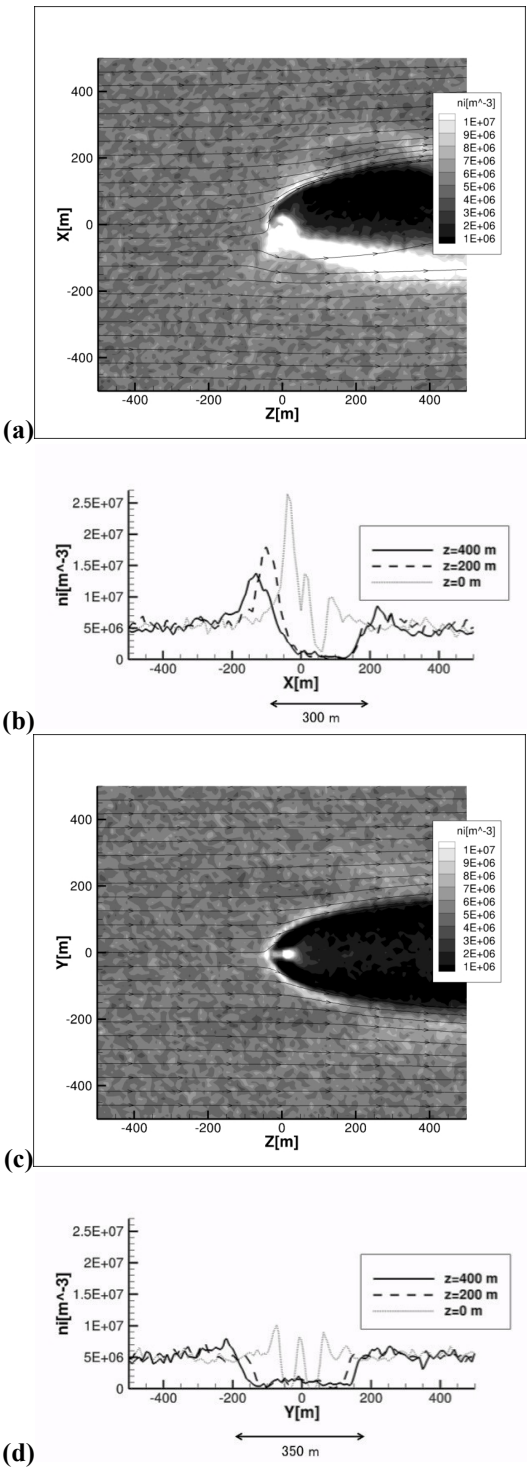

Fig. 5 Ion density distribution in the perpendicular case across (a) the xz-plane (y = 0 m) and (c) the yz-plane (x = 0 m). One-dimensional cuts along the x-axis (y=0 m and z=0 m, 200 m, 400 m) and the y-axis (x=0 m, z=0 m, 200 m, 400 m) are also shown in (b) and (d) (M = 1.3 × 10^8 Wb·m, typical solar wind).

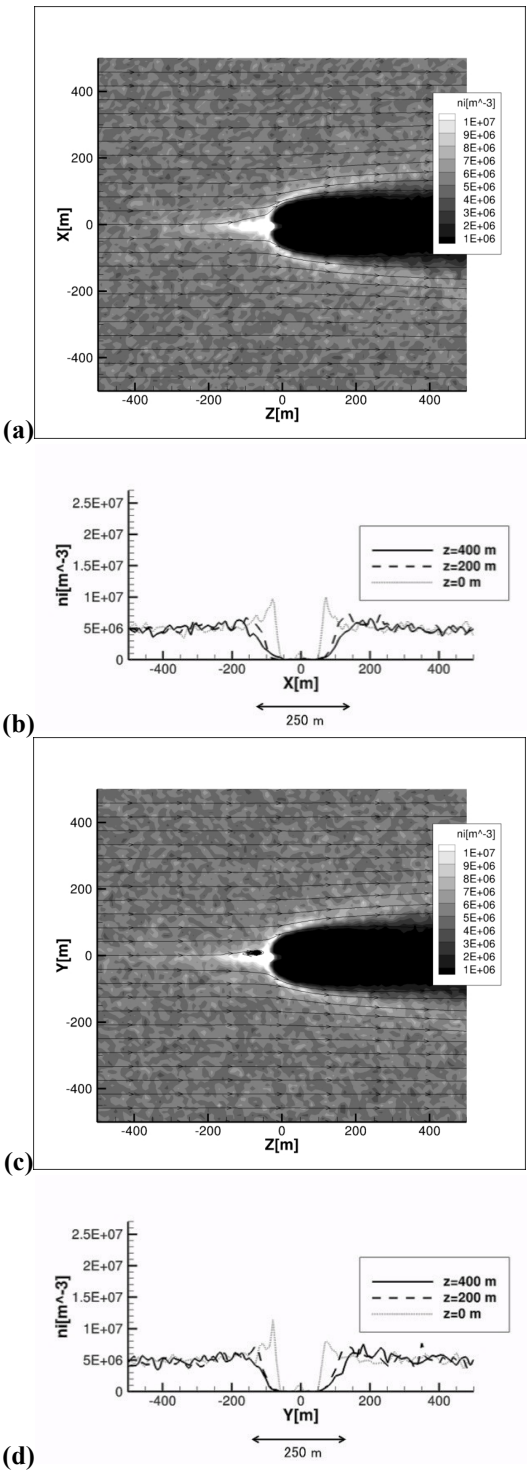

Fig. 6 Ion density distribution in the parallel case across (a) the xz-plane (y = 0 m) and (c) the yz-plane (x = 0 m). One-dimensional cuts along the x-axis (y=0 m and z=0 m, 200 m, 400 m) and the y-axis (x=0 m, z=0 m, 200 m, 400 m) are also shown in (b) and (d) (M = 1.3 × 10^8 Wb·m, typical solar wind).

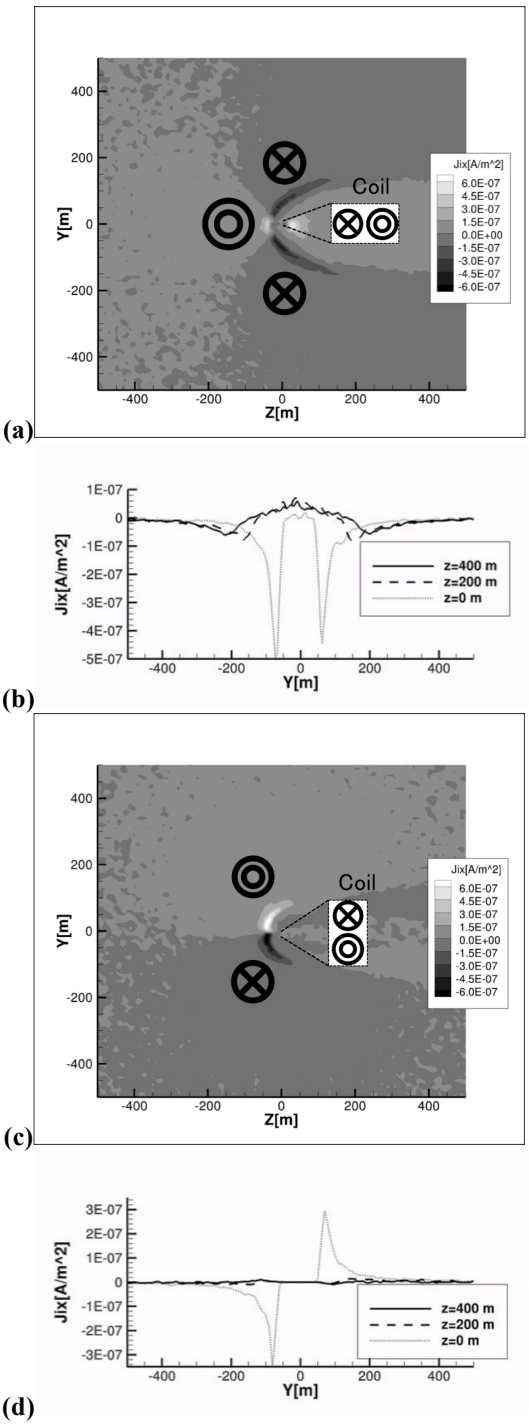

Fig. 7 Current density distribution in the perpendicular case (a) and the parallel case (b) across the yz-plane (x = 0). The direction of the onboard coil current is also represented ($M = 1.3 \times 10^8$ Wb·m, typical solar wind).

B. Thrust for various values of the design parameter, magnetic moment *M*

The thrust of the magnetic sail was investigated for various different values of the design parameter (the magnetic moment of the onboard coil, M). Simulations were performed by changing the magnetic moment M from 1.3×10^6 Wb·m to 1.3×10^{11} Wb·m in six steps for both the both perpendicular case and the parallel case. In total, 12 simulation cases were carried out. It takes about 4 days (1024 CPUs) per case to obtain the steady states of smaller plasma cavities ($M<1.3 \times 10^{10}$ Wb·m); whereas it takes one week (4096 CPUs) for larger plasma cavities ($M>1.3 \times 10^{10}$ Wb·m), since a computational domain of 512 × 512 × 512 cells is required. Figure 8 shows the results. The relationship between the magnetic moment and the thrust was fitted by the least-squares method. This revealed that the thrust of a small-scale magnetic sail is approximately proportional to the magnetic moment of the onboard coil ($F \propto M$).The simulation results from hybrid-PIC simulation [4] are also plotted in Fig. 8. The thrust obtained by the Full-PIC simulation is two or three times larger than the thrust obtained by hybrid-PIC simulation, which neglects the electron kinetic effects by assuming a massless electron fluid. Because of the finite Larmor radius effect of electron, which is one of the electron kinetic effects, the drift velocity and the magnetopause current in the non-uniform electromagnetic field around the magnetopause become larger. As a result, the thrust of a magnetic sail with a small plasma cavity becomes larger if we take the electron kinetic effects into consideration. This shows that electron kinetic effects that are ignored in simulation methods other than full-PIC simulations become dominant in small-scale plasma cavities and affect the thrust characteristics of small-scale magnetic sails.

The thrust characteristics ($F \propto M$) are clearly different from the thrust characteristics of larger magnetic sails as obtained by hybrid-PIC simulations [4], flux tube simulations [7] and MHD simulations ($F \propto M^{2/3}$) [3] as shown in Fig. 9. The lines which are extrapolated from the full-PIC result and the MHD result cross for M~1.0×10^{13} Wb·m, where the magnetosphere size L_{MHD} ~20 km is much smaller than the ion Larmor radius (typically 100 km). It is therefore expected that the kinetic effects of ions also have strong influence on the thrust characteristics of magnetic sails with a small plasma cavity ($L_{\mathrm{MHD}}<R_{\mathrm{iL}}$).

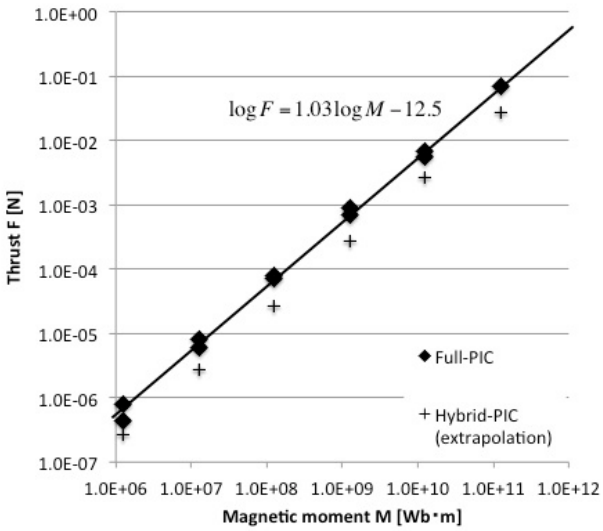

Fig. 8 Thrust characteristics of magnetic sails of various magnetic moments obtained by three-dimensional simulation (typical solar wind, α = 0 deg and 90 deg).

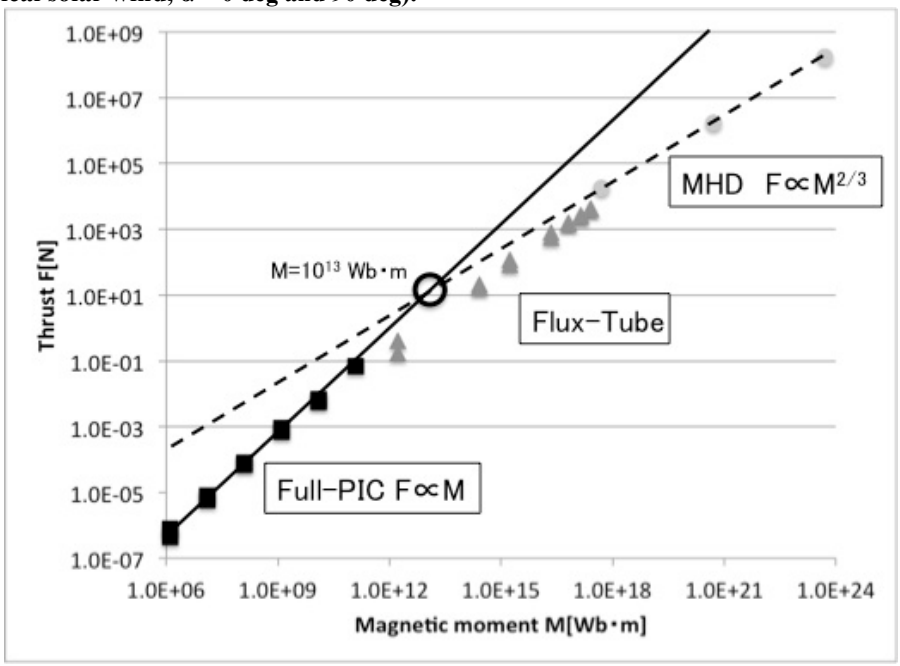

Fig. 9 Thrust characteristics of small (full-PIC) to large (MHD) magnetic sails.

C. Thrust under various solar wind parameters

Next, we performed nine simulations assuming changes in the solar wind parameters, specifically the number density N_{SW} and plasma velocity V_{SW}. No previous study has taken the variation of the solar wind into consideration. However, for deep space exploration, the thrust characteristics of a magnetic sail in interplanetary space have to be determined and these are likely to change since the solar wind will vary spatially and temporally along the spacecraft's trajectory. The solar wind density was set to 0.5, 1 and 2 times the typical value, and the velocity was

similarly set to 0.5, 1 and 2 times the typical value, where the typical solar wind parameters are listed in Table 1. The magnetic moment M and other design parameters of the magnetic sail are fixed at the values listed in Table 2.

Figure 10 shows the results for each set of solar wind parameters. The thrust of the magnetic sail increases as the velocity and the density of the solar wind increase. This is because the dynamic pressure of the solar wind ($\sim 0.5 m_i N_{SW} V^2_{SW}$) becomes larger. The relationship between the velocity V_{SW}, density N_{SW} and thrust was fitted using the least-squares method. This found that the thrust of the magnetic sail changes approximately in proportion to the changes in V_{SW} and N_{SW}, as given by the following relation:

$$F \propto V_{SW}^{0.92} \times N_{SW}^{1.15} \tag{6}.$$

The thrust is slightly more sensitive to changes in density than velocity. Due to the fast flow velocity, that is, large Larmor radius, the contribution of ions to the magnetic field becomes large and, as mentioned below, the plasma cavity becomes smaller. As a result, the thrust of magnetic sail cannot become as large as expected from the increase in the dynamic pressure.

The plasma density of the solar wind N_{SW} is assumed to be inversely proportional to the square of the Sun–spacecraft distance ($N_{SW} \propto |\mathbf{R}|^{-2}$) and the velocity V_{SW} is assumed to be constant in interplanetary space. The thrust of a small-scale magnetic sail is therefore inversely proportional to the 2.3 power of the Sun–spacecraft distance ($F \propto N_{SW}^{-1.15} \propto |\mathbf{R}|^{-2.3}$). Magnetic sails, therefore, differ in their thrust characteristics from existing propulsion systems, for example, a solar sail ($F \propto |\mathbf{R}|^{-2}$). That is, in outer planet orbits, the thrust of a magnetic sail would be smaller than that of a solar sail even if the thrust level is the same in Earth orbit. On the other hand, the thrust of a magnetic sail is larger in inner planet orbits.

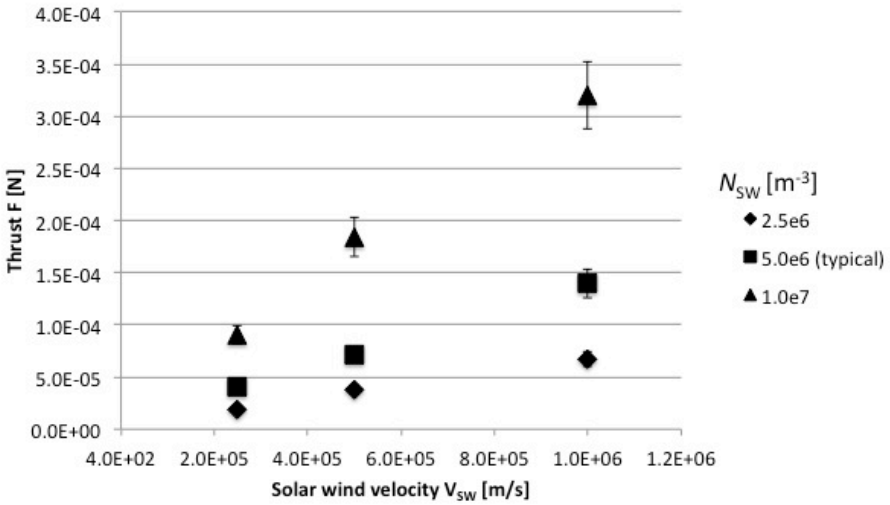

Fig. 10 Thrust characteristics of a magnetic sail under various solar wind parameters (solar wind velocity V_{SW} and density N_{SW}) obtained by three-dimensional simulation (M = 1.3 × 10^8 Wb·m, parallel case).

D. Thrust and steering angle β under various attack angles α

Simulations were performed at various attack angles α in order to investigate the effect on thrust of the correlation between the solar wind and the design parameters of the magnetic sail. In addition to the dipole magnetic field assumed in previous simulations, we also investigated magnetic fields generated by coils of 50 m and 100 m in diameter. The magnetic moment is kept constant at 1.3 × 10^8 Wb·m.

The results are shown in Figs. 11, 12 and 13. In Figure 11 it can be seen that, as the attack angle α increases, the thrust of the magnetic sail also increases. This is because the cross-sectional area of the plasma cavity changes with attack angle as shown in Figs. 5 and 6. These characteristics are in agreement with previous studies on large magnetospheres [18, 19]. This relationship between attack angle α and thrust is common to all scales. In addition, the thrust decreases as the coil radius increases (Fig. 12), because solar wind plasma is able to pass through the center of a coil without undergoing mirror reflection even if the magnetic moment is the same. The density distribution and the streamlines of the solar wind are shown in Fig. 14 when the coil axis is parallel to the solar wind direction. When the coil radius is comparable with the size of the plasma cavity, the interaction between the magnetic field and the solar wind occurs only near the coil and the thrust decreases by 40% compared with the thrust of the ideal dipole. To approximate the thrust of a dipole, the coil radius needs to be less than 20 m (1/5 of size of the plasma cavity).

In contrast, the steering angle β increases as the coil radius increases, peaking at α = 45 deg, as shown in Fig. 13. The steering angle β represents the angle in the yz-plane when the attack angle α is in the neighborhood of 0 deg and the angle in the xz-plane when the attack angle α is in the neighborhood of 90 deg. Only the angle between the thrust vector and the solar wind direction (anti-sunward direction or orbital-radius direction) affects the orbital change capability of a small-scale magnetic sail as we show in the next section. We, therefore, do not distinguish of the steering angle from the plane containing the thrust vector.

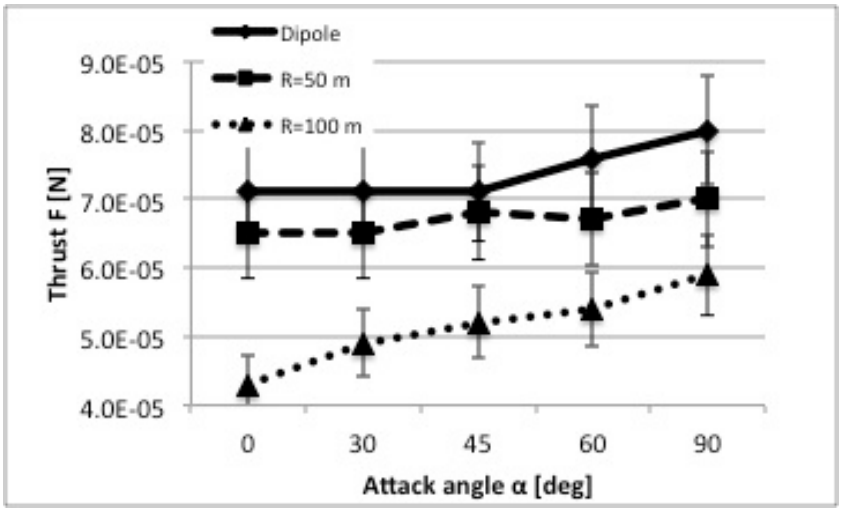

Fig. 11 Thrust characteristics of a magnetic sail at various attack angles α as obtained by three-dimensional simulation ($M = 1.3 \times 10^8$ Wb·m, typical solar wind).

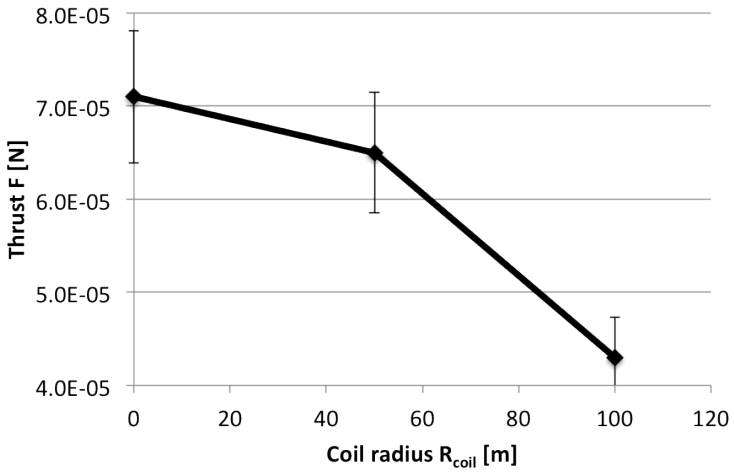

Fig. 12 Thrust for various coil sizes (M = 1.3 × 10^8 Wb·m, typical solar wind, α=0 deg).

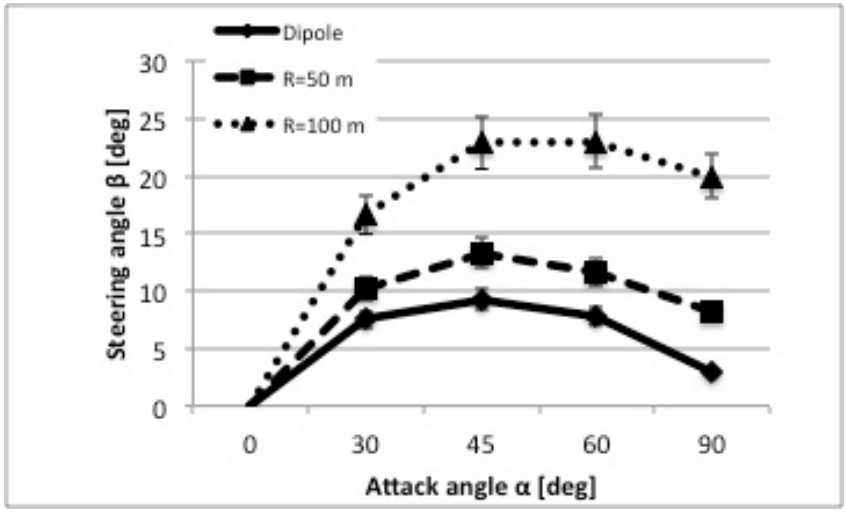

Fig. 13 Steering angle β characteristics of a magnetic sail at various attack angles α as obtained by three-dimensional simulation (M = 1.3 × 10^8 Wb·m, typical solar wind).

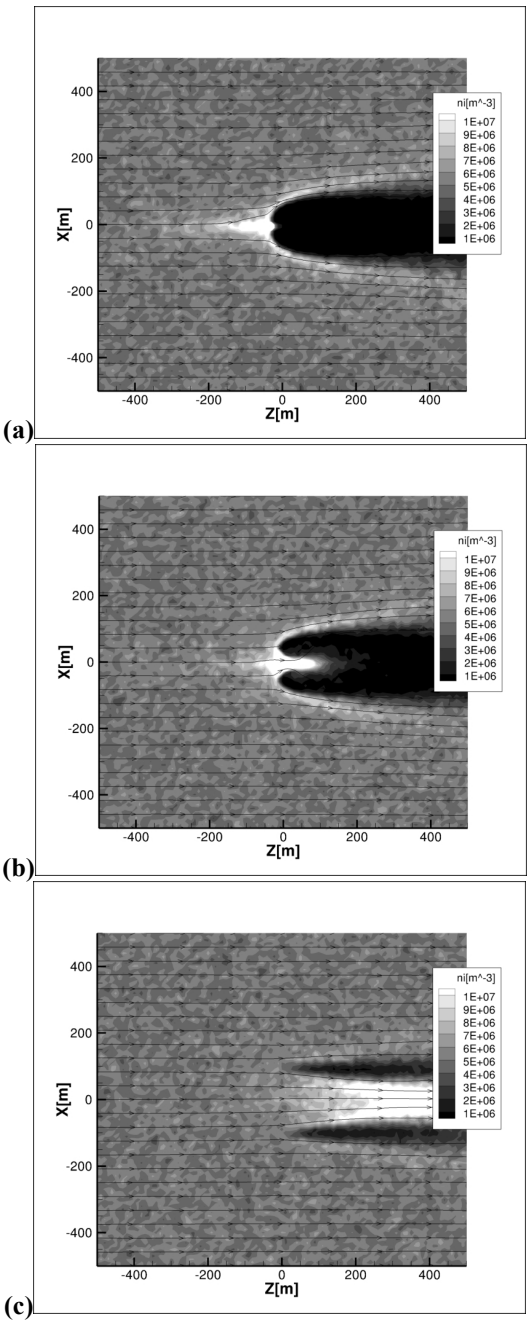

Fig. 14 Ion density distribution and streamlines with various coil sizes: (a) ideal dipole, (b) R_{coil} = 50 m and (c) R_{coil} = 100 m (M = 1.3 × 10^8 Wb·m, parallel case α = 0 deg, typical solar wind).

IV. Discussion

A. Summary of thrust characteristics and theoretical validation

As discussed above, we performed large three-dimensional full-PIC simulations by using parallel computing techniques and huge computational resources. We found that the thrust of a small-scale magnetic sail is determined by the magnetic moment M of the onboard coil (main design parameter of the spacecraft), the solar wind parameters (density N_{SW} and velocity V_{SW}) and the attack angle α. Combining these results and assuming no cross-correlation between parameters gives empirical formulae for the thrust F and steering angle β:

$$F = 3.57\times10^{-26} N_{SW}^{1.15} V_{SW}^{0.92} M^{1.03} \left(1.55\times10^{-3}\alpha + 1\right) \quad (1.3\times10^{6} < M < 1.3\times10^{11}) \tag{7}$$

and

$$\beta = -3.60\times10^{-3}\left(\alpha - 50\right)^{2} + 9.01 \tag{8}.$$

These equations show that the thrust of a small-scale magnetic sail is approximately proportional to magnetic moment, solar wind density and solar wind velocity. In addition, it is revealed that the magnetic sail can generate not only radial thrust but also a tangential thrust that is effective for accelerating the spacecraft along its trajectory.

This thrust characteristics of magnetic sail were also examined theoretically. We first performed a test-particle simulation using only a dipole magnetic field, which neglects the time variation of the electromagnetic field. The test-particle simulation takes only the interaction between ions and the coil magnetic field into consideration and the electrostatic field due to the charge separation is neglected. Figure 15 shows a schematic illustration of the interactions between ion, electron and magnetic field included in the test-particle and full-PIC simulations. The induced magnetic field is far smaller than the coil magnetic field. As shown in Fig. 16, the plasma cavity with almost same structure as that of full-PIC simulation was formed in the test-particle simulation. The test-particle simulation approximately reproduces the momentum change of ions, but cannot reproduce the electromagnetic force acting on the superconductive coil onboard spacecraft since the current induced by electrons is strongly affected by the electron kinetics. It was found that the cross-sectional area of the magnetic sail is mainly formed by the interaction between ions and the dipole magnetic field, and electrons hardly influence the structure of the plasma cavity but do induce the magnetopause current.

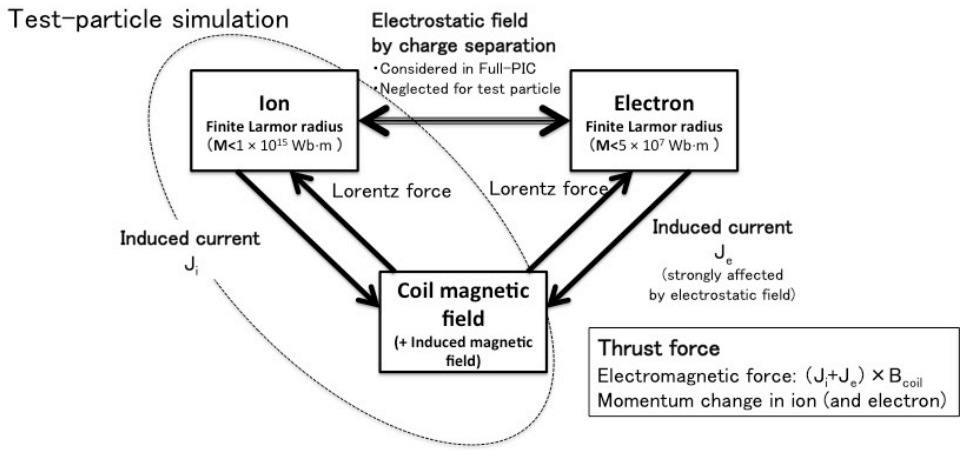

Fig. 15 Schematic illustration of interaction between ion, electron and magnetic field.

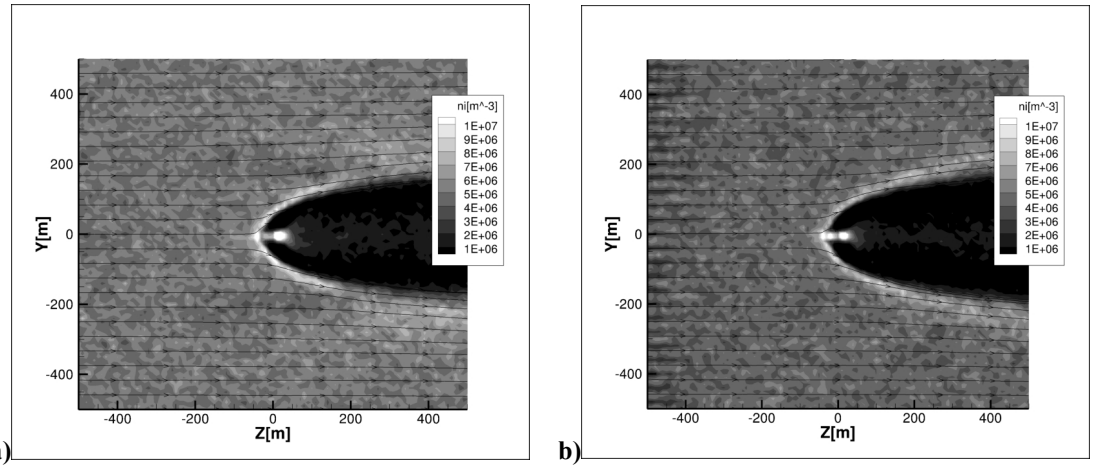

Fig. 16 Ion density distribution obtained by (a) full-PIC simulation and (b) test particle simulation ($M = 1.3 \times 10^8$ Wb·m, perpendicular case $\alpha = 90$ deg, typical solar wind).

Hence, we estimated the size of the plasma cavity theoretically by considering only ion trajectories in a dipole magnetic field. We considered the xz-plane, as shown in Fig. 17. The vector potential

$$\left(A_x, A_y\right) = \left(\frac{\mu_0 M_y z}{4\pi r^3}, \frac{\mu_0 M_y x}{4\pi r^3}\right) \tag{9}$$

is defined using the magnetic moment M. Conservation of the generalized momentum of a particle which has velocity (0, V_{SW}) at infinity is used. At the stagnation point (0, -L_s), the particle should have the velocity (V_{sw}, 0) because of the conservation of energy and Larmor motion. The conservation of the generalized momentum along the x-axis is represented as

$$0 = m_i V_{SW} - \frac{e\mu_0 M}{4\pi}\frac{L_s}{L_s^3} \tag{10}.$$

Solving for the plasma cavity size yields

$$L_s = \sqrt{\frac{e\mu_0 M}{4\pi m_i V_{SW}}} \tag{11}$$

The plasma cavity size obtained by full-PIC simulation, L_s from Eq. (11) and the magnetosphere size L_{MHD} (Eq. (1)) that is obtained by MHD approximation are compared in Fig. 18. It can be seen that the plasma cavity size obtained by single particle approximation is in good agreement with the full-PIC simulation results ($M > 5 \times 10^7$ Wb·m) and the MHD approximation is not valid at all on the kinetic scale. For smaller magnetic moments ($M < 5 \times 10^7$ Wb·m), the plasma cavity size obtained by full-PIC is larger than the plasma cavity size expected from Eq. (11), since the electron kinetics and charge separation become strong when the plasma cavity size, electron Larmor radius and Debye length are comparable. The MHD approximation L_{MHD} and the theoretical result L_s agree for $M = 1.0\times 10^{15}$ Wb·m, which corresponds to a magnetosphere of size L=140 km. When the magnetosphere size or the plasma cavity size is larger than the ion Larmor radius (typically 100 km), the MHD approximation is expected to be valid as it is in the field of geophysics.

The cross-sectional area of the plasma cavity can therefore be approximately estimated as being πL_s^2. Since the magnetic sail catches the solar wind's dynamic pressure with this cross-sectional area, the thrust is approximately given by

$$F = \frac{1}{2} m_i N_{SW} V_{SW}^2 \times \pi \frac{e\mu_0 M}{4\pi m_i V_{SW}} = 2.5 \times 10^{-26} N_{SW} V_{SW} M \quad (12).$$

The coefficient and indices of Eq. (12) are in reasonable agreement with those of Eq. (7). The validity of the thrust characteristics based on simulation results is thus supported by theoretical arguments.

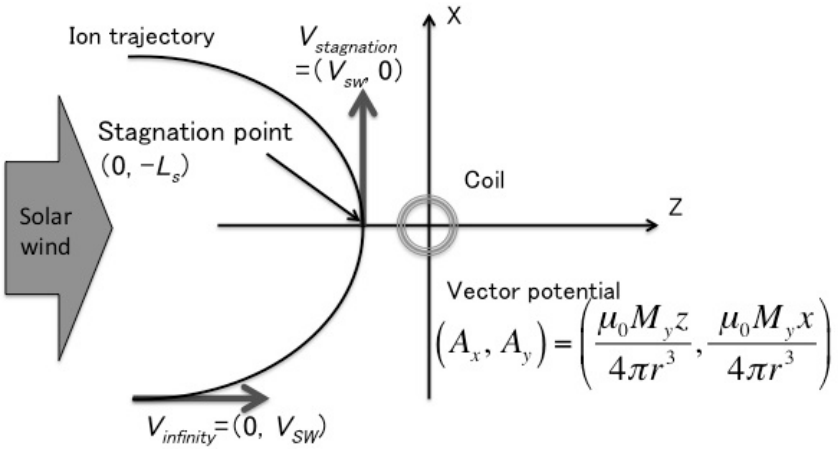

Fig. 17 The definition of axes in the theoretical estimation of plasma cavity size L_s.

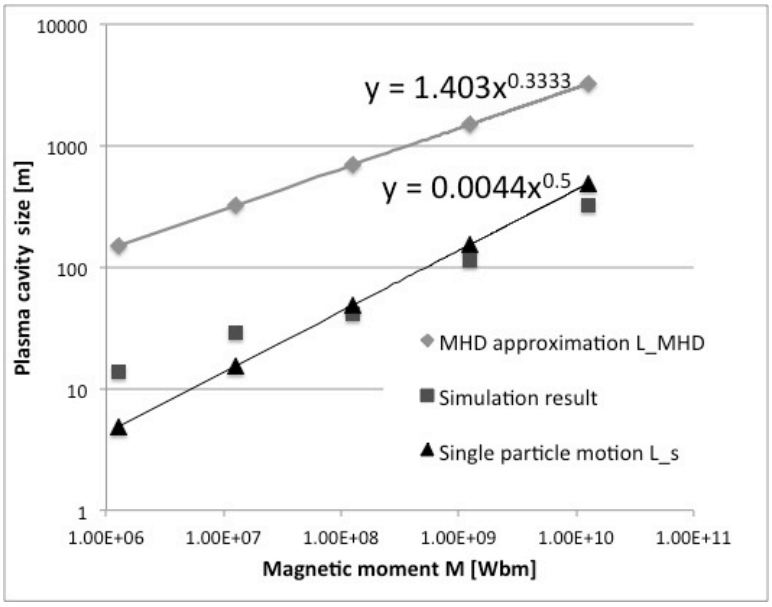

Fig. 18 Comparison of plasma cavity sizes from simulation and theoretical analysis.

B. Evaluation of thrust-mass ratio

By using the empirical formulae for the thrust characteristics of small-scale magnetic sails, the trajectory of a magnetic sail spacecraft can be determined and mission analysis attained can be achieved. Although the mission analysis of large-scale magnetic sails (ion scale ~ MHD scale, which are unrealizable with present technology) has already been conducted [20], the kind of the mission for which a small-scale magnetic sail is suitable has not been determined.

First, we calculated the thrust-mass ratio of a small-scale magnetic sail by using a feasible design for the magnetic sail and the thrust characteristics we have found. Table 3 shows magnetic sail design parameters that are

feasible with present technology and Table 4 shows the properties of the superconducting material we assumed in order to estimate the coil weight. A thrust of 6.5 μN can be generated using a 200 kg superconducting coil. That is, the thrust-mass ratio is 3.3×10^{-5} mN/kg. The thrust-mass ratio of a small-scale magnetic sail is thus much smaller than that of other existing propulsion systems, such as solar sails (0.07 mN/kg of IKAROS) and ion engines (0.40 mN/kg of HAYABUSA and 1.9 mN/kg of Deep Space 1, if we consider only the thrust system without fuel). In addition, the weight of the coil cooling system and the electric power supply system should be considered for a more exact comparison with existing propulsion systems. This result shows that the thrust of a small-scale magnetic sail that is feasible with present technology is insufficient for deep space exploration and an increase in the thrust by using new technology, such as a Magneto Plasma Sail, is required.

On the other hand, a magnetic sail can be used for a maneuvering system to maintain a halo orbit at the Sun-Earth Lagrangian points. Orbit maintenance requires only low thrust (total delta v of approximately a few meters per second per year [21]), and the required thrust generation and control of thrust direction by a small-scale magnetic sail can be achieved even with present technology. Formation flight in a halo orbit or in interplanetary space is also candidate use for the magnetic sail. When the thrust of the magnetic sail is always in the anti-sunward, a new periodic orbit appears around a halo orbit (Sun-Earth L1 and L2) [22]. For the conditions above (3.3×10^{-5} mN/kg thrust-mass ratio), the interval between the two orbits is approximately 100 km, and a large-sized structure, such as space telescope can be constructed by formation flight without consuming fuel. It may also be possible to use a magnetic sail to control an orbit and attitude effectively over a long period of time by taking advantage of the characteristic that the specific impulse is infinite and the amount of electric power required is very small due to the use of a superconducting coil.

It is also expected that the thrust-mass ratio could be made 2~5 times better than the results of this study through improvements in superconducting technology and an optimal design of the superconductive coil for a magnetic sail [23, 24]. The use of a plasma jet (M2P2/MPS concept) as proposed by Winglee et al. [2], the use of dipole plasma equilibrium to inflate the magnetic field (ring-current concept) as proposed by Funaki et al. [25] and the use of a rotating magnetic field (plasma magnet concept) as proposed by Slough et al. [26] should be also analyzed by full-PIC simulation in three dimensions since previous research neglecting electron kinetics failed to demonstrate an improvement of thrust performance. To achieve deep space exploration by magnetic sail, it is also necessary not only to improve the thrust level of the magnetic sail but also to improve the controllability of the thrust vector by

using a larger coil, as described in section III.D. In addition, it is necessary to optimize the spacecraft trajectory by controlling the thrust vector dynamically [27, 28]. To do this, attitude stability has to be analyzed as well as the thrust characteristics. These problems are left as work for the future because of the very complicated analysis conditions and huge computational load.

Table 3 Magnetic sail design parameters

R_{coil} [m]	2.0
Coil current [A turn]	1.0×10^6
Magnetic moment [Wb·m]	1.3×10^7
Coil weight [kg]	200

Table 4 Properties of superconducting material

Type	BSCCO
Width [mm]	4.3
Thickness [mm]	0.23
Density [g/cm^3]	10
Critical Current [A]	500

V. Conclusion

We performed three-dimensional full-PIC simulations in order to determine the thrust characteristics of small-scale magnetic sails. It was found that the thrust level of the magnetic sail is approximately proportional to the magnetic moment of the onboard coil, solar wind density and solar wind velocity. This is quite different from large magnetic sails since particle motion is the dominant influence on thrust generation in small-scale magnetic sails. It was also found that the attack angle and coil radius affect the steering angle and that the steering angle increases (up to a maximum of 20 deg) as the coil radius increases.

Finally, we evaluated the thrust-mass ratio of a small-scale magnetic sail using the thrust characteristics obtained from the full-PIC simulations. The results showed that the thrust of a small-scale magnetic sail is insufficient for deep space exploration. However, the consequences of the use of thrust improvement techniques, such as plasma injection, remain to be analyzed. In order to achieve fast interplanetary flight for deep space exploration, increased thrust from a magneto plasma sail is needed. Optimization of the magnetic sail orbit through the ability to turn the coil on and off and by control of the steering angle is also needed. This is left as work for the future.

Acknowledgments

Some computations in the present study were performed using the K computer at RIKEN (Number hp120084), the Kyoto-daigaku Denpa-kagaku Keisanki-jikken system of the Research Institute for Sustainable Humanosphere at Kyoto University and the JAXA Supercomputing System (JSS) as a collaborative research project. We gratefully acknowledge the support and advice of the members of the Magneto Plasma Sail Research Group in Japan. This work has also been supported by Core Research for Evolutional Science and Technology (CREST) of the Japan Science and Technology Agency (JST) and JSPS KAKENHI Grant Number 241626.

References

[1] Zubrin, R. M., and Andrews, D. G., "Magnetic Sails and Interplanetary Travel," *Journal of Spacecraft and Rockets*, Vol. 28, No. 2, 1991, pp.197-203.

[2] Winglee, R. M., Slough, J., Ziemba, T., and Goodson, A., "Mini-Magnetospheric Plasma Propulsion: Trapping the Energy of the Solar Wind for Spacecraft Propulsion," *Journal of Geophysical Research*, Vol. 105, 2000, pp. 21067-21077.

[3] Nishida, H., Ogawa, H., Funaki, I., Fujita, K., Yamakawa, H., and Inatani, Y., "Verification of Momentum Transfer Process on Magnetic Sail Using MHD Model," 41st AIAA/ASME/SAE/ASEE Joint Propulsion Conference and Exhibit, Tucson, Arizona, Paper 2005-4463, Jul, 2005.

[4] Fujita, K., "Particle Simulation of Moderately Sized Magnetic Sails," *Journal of Space Technology and Science*, Vol. 20, No. 2, 2005, pp. 26-31.

[5] Kajimura, Y., Usui, H., Funaki, I., Ueno, K., Nunami, M., Sinohara, I., Nakamura, N. and Yamakawa, H., "Hybrid Particle-in-Cell Simulations of Magnetic Sail in Laboratory Experiment," *Journal of Propulsion and Power*, Vol. 26, No. 1, 2010, pp. 159-166.

[6] Ueno, K., Kimura, T., Ayabe, T., Funaki, I., Yamakawa, H. and Horisawa, H., "Thrust Measurement of Pure Magnetic Sail", ISTS, Hamamatsu, Japan, 2008-b-05, 2008.

[7] Ashida, Y., Funaki, I., Yamakawa, H., Kajimura, Y. and Kojima, H., "Thrust Evaluation of a Magnetic sail by Flux-Tube Model," *Journal of Propulsion and Power*, Vol. 28, No. 3, 2012, pp. 642-651.

[8] Nishida, H., Funaki, I., Ogawa, H. and Inatani, Y., "MHD Analysis on Propulsive characteristics of Magneto Plasma Sail," 30th International Electric Propulsion Conference, Florence, Italy, IEPC-2007-195, Sep, 2007.

[9] Saha, S., Singh, N., Craven, P., Gallagher, D., and Jones, J., "Development of 3D Hybrid Code and Its Application to M2P2," Space Technology and Applications International Forum-STAIF 2002, Albuquerque, NM, 2001, pp. 441-446.

[10] Winske, D. and Omidi, N., "Plasma expansion in the presence of a dipole magnetic field," *Physics of Plasmas*, Vol. 12, 2005, pp. 072514-1-12.

[11] Omidi, N. and Karimabadi, H., "Kinetic Simulation/Modeling of Plasma Sail," 39th AIAA/ASME/SAE/ASEE Joint Propulsion Conference and Exhibit, Huntsville, Alabama, Paper 2003-5226, Jul, 2003.

[12] Kajimura, Y., Funaki, I., Shinohara, I., Usui, H. and Yamakawa, H., "Thrust Evaluation of Magneto Plasma sail by Using Three-Dimensional Hybrid PIC Code," 46st AIAA/ASME/SAE/ASEE Joint Propulsion Conference and Exhibit, Nashville, Tennessee, AIAA-2010-6686, 2010.

[13] Pfeiffer, M., Petkow, D., Herdich, G. and Fasoulas, S., "Assesment of a Numerical Approach Suitable for the M2P2 Problem," *The Open Plasma Physics Journal*, Vol. 4, 2011, pp. 24-33.

[14] Moritaka, T., Kajimura, Y., Usui, H., Matsumoto, M., Matsui, T. and Shinohara, I., "Momentum transfer of solar wind plasma in a kinetic scale magnetosphere," Physics of Plasmas, Vol. 19, 2012, pp. 032111-1-13.

[15] Ashida, Y., Funaki, I., Yamakawa, H., Usui, H., Kajimura, Y. and Kojima, H., "Two-Dimensional Particle-In-Cell Simulation of Magnetic Sails," *Journal of Propulsion and Power*, accepted.

[16] Parks, G. K., *Physics of Space Plasmas*, 2nd Ed., Westview Press, Boulder, CO, 2004, pp. 355-362.

[17] Matumoto, H. and Omura, Y., *Computer Space Plasma Physics*, Terra Scientific Publishing Company, Tokyo, Japan, 1993, pp. 37-41.

[18] Nishida, H. and Funaki, I., "Analysis of Thrust Characteristics of a Magnetic Sail in Magnetized Solar Wind," *Journal of Propulsion and Power*, Vol. 28, No. 3, 2012, pp. 336-642.

[19] Kajimura, Y., Funaki, I., Matsumoto, M., Shinohara, I., Usui, H. and Yamakawa, H., "Thrust and Attitude Evaluation of Magnetic Sail by Three-dimensional Hybrid Particle-in-Cell Code," *Journal of Propulsion and Power*, Vol. 28, No. 3, 2012, pp. 652-663.

[20] Quarta, A. A., Mangali, G. and Aliasi, G., "Optimal control law for heliocentric transfers with a magnetic sail," *Acta Astronautica*, Vol. 89, 2013, pp. 216-225.

[21] Roberts, C. E., "The SOHO mission L1 Halo Orbit Recovery from the Attitude Control Anomalies of 1998," *Libration Point Orbits and Applications: Proceedings of the Conference*, world scientific publishing company, Singapore, 2003, pp. 171-218.

[22] Morimoto, M., Yamakawa, H. and Uesugi, K., "Periodic orbits with Low-Thrust Propulsion in the Restricted Three-body Problem," *Journal of Guidance, Control and Dynamics*, Vol. 29, No. 5, 2006, pp.1131-1139.

[23] Nagasaki, Y., Nakamura, T., Funaki, I., Ashida, Y. and Yamakawa, H., "Conceptual Design of YBCO Coil with Large Magnetic Moment for Magnetic Sail Spacecraft," *IEEE Trans. Appl. Supercond*. Vol. 23, No. 3, 2013, pp. 4603405.

[24] Nagasaki, Y., Nakamura, T., Koyama, T., Funaki, I., Ashida, Y., Kojima, H. and Yamakawa, H., "Characteristic comparison between Bi-2223/Ag and YBCO system superconducting magnets for magnetic sail spacecraft," Asian Conference on Applied Superconductivity and Cryogenics 2011, New Delhi, India, P-122, Nov, 2011.

[25] Funaki, I., Kajimura, Y., Ashida, Y., Nishida, H., Oshio, Y., Shinohara, I. and Yamakawa, H., "The Use of Dipole Plasma Equilibrium for Magnetic Sail Spacecraft", *Transactions of Fusion Science and Technology*, Vol.63, No. 1T, 2013, pp. 168-171.

[26] Slough, J., "Plasma Sail Propulsion Based on the Plasma Magnet," 30th International Electric Propulsion Conference, Florence, Italy, IEPC-2007-15, Sep, 2007.

[27] Yamakawa, H., "Dynamics of Radially Accelerated Trajectories," *Transactions of the Japan Society for Aeronautical and Space Sciences*, Vol. 49, No. 164, 2006, pp. 77-80.

[28] Yamakawa, H., "Optimal Radially Accelerated Interplanetary Trajectories," *Journal of Spacecraft and Rockets*, Vol. 43, No. 1, 2006, pp. 116-120.